Characterization of Low Lewis Number Flames

A. J. Aspden, M. S. Day and J. B. Bell

Lawrence Berkeley National Laboratory, Berkeley, CA 94720, USA

Abstract

A recent numerical study of turbulence-flame interactions in lean premixed hydrogen, where the Lewis number was approximately 0.36, observed that flames at different equivalence ratios presented significantly different behavior despite having the same Karlovitz and Damköhler numbers. This differing behavior is due to the thermodiffusively-unstable nature of low Lewis number flames. In more than one dimension, differential diffusion focuses fuel into hot regions increasing the local burning rate, which was found to affect the leaner hydrogen flames more significantly. Ultimately, this difference between idealized flat flames and freely-propagating flames undermines the characterization of turbulent flames through Karlovitz and Damköhler numbers based on flat laminar quantities. This paper considers refining the definitions of these dimensionless numbers by replacing the flat laminar flame values with freely-propagating values. In particular, we perform three-dimensional simulations of freely-propagating flames over a range of equivalence ratios, and use data from those simulations to define modified Karlovitz and Damkölher numbers. We then perform a series of turbulent flame simulations that show that defining Karlovitz and Damkölher numbers based on the freely-propagating flames effectively eliminates dependence on equivalence ratio.

1. Introduction

There has been considerable recent interest in hydrogen or hydrogen-rich mixtures obtained from gasification of coal or biomass as alternatives to petroleum. Burning under lean conditions reduces the exhaust gas temperatures, and consequently, thermal NO_x emissions. At the low to moderate levels of turbulence, the thermodiffusive instability of H_2 flames leads to flames that burn in well-known cellular structures, going back to early work by Markstein [1] and Zeldovich [2]. Cellular burning patterns have been observed experimentally in lean H_2/O_2 mixtures by many researchers (see, for example, [3] and [4]). Low-swirl burner technology, introduced by [5], has proven to be an effective stabilization mechanism for a wide range of fuels, including H_2, see [6] and [7]. Turbulent lean H_2 flames at moderate turbulence levels have also been studied computationally, both in idealized configurations by [8–10], and in a low-swirl burner configuration [11]. These simulations show that the thermodiffusive instability leads to localized hot spots where the flame is burning more intensely because of local enrichment of the fuel by diffusion. However, realistic turbine combustors often reach much higher levels of turbulent intensity, e.g. [12] measured turbulent intensities as high as 30 m/s.

Little is known about the behavior of H_2 flames in high intensity turbulence; particularly, what role the high diffusivity of H_2 plays. Aspden *et al.* [13] considered turbulence-flame interactions in lean premixed hydrogen in an idealized setting that will be described in detail in section 4. For the range of equivalence ratios studied, $\varphi = 0.31\text{-}0.40$, the Lewis number is in the approximate range 0.35 to 0.365. The dimensionless Karlovitz and Damköhler numbers

$$\text{Ka}_L^2 = \frac{\check{u}^3}{s_L^3}\frac{l_L}{l} \quad \text{and} \quad \text{Da}_L = \frac{s_L}{\check{u}}\frac{l}{l_L}$$

were used to normalize the simulations, where $\check{u}$ and l are the turbulent rms velocity and integral length scale, respectively, and s_L and l_L are the flat laminar flame speed and width, respectively. To investigate the effect of equivalence ratio, simulations were configured to have the same Ka_L and Da_L (by fixing the turbulent conditions according to laminar flame properties, i.e. $\check{u} \propto s_L$, and $l \propto l_L$). Despite this normalization, flames at different equivalence ratios presented very different behavior, even to the extent of different burning regimes. An example is shown in figure 1, which presents two-dimensional slices through three-dimensional simulations of lean premixed hydrogen under highly turbulent conditions (these cases are denoted D31 for $\varphi = 0.31$ through D40 for $\varphi = 0.4$). The flames are propagating downwards in a high aspect ratio (8:1) domain with a maintained background turbulent velocity field. Slices of density, burning rate, and temperature are shown for four equivalence ratios at $\text{Ka}_L \approx 1560$ and $\text{Da}_L \approx 0.0047$. It is clear that the flame responds very differently to the scaled turbulence in each case. At the low

equivalence ratio, there is a sharp interface between fuel and products, the turbulence is unable to disrupt the internal structure of the flame, and the burning occurs in small-scale structures across a broad flame brush. This case is burning in the thin reaction zone regime. As the equivalence ratio was increased (keeping both Ka_L and Da_L fixed), it was found that the turbulence increasingly disrupted the internal flame structure. At $\varphi = 0.4$, there was a single turbulently-broadened flame, where there was no longer a sharp interface between the fuel and products, and the burning occurred at the high temperature end of the flame. This flame is burning in the distributed burning regime (see [13] for more details).

This is counter-intuitive at first, as it should be expected that the slower thicker flame ($\varphi = 0.31$) should become distributed more easily. However, this was accounted for by normalizing the turbulence by the laminar flame properties, so it should be expected that the flame response should be similar in each case. It appears that for low Lewis number flames, the shift from laminar to turbulent flames is not only affected by the turbulence, but also the equivalence ratio. [13] suggested that this disparity is an artifact of the low Lewis number and associated thermodiffusive instability, because preferential diffusion of fuel can enhance the local flame speed, which has a greater effect at lower equivalence ratio. This suggests that the Karlovitz number and Damköhler number based on laminar values do not accurately capture the effect of turbulence on low Lewis number flames.

This paper proposes to rectify this shortcoming by replacing the laminar flame properties with freely-propagating values that provide a more accurate reflection of the flame speed and width that the turbulence is competing with. These freely-propagating values can then be used to construct modified Karlovitz and Damköhler numbers

$$\text{Ka}_F^2 = \frac{\check{u}^3}{s_F^3}\frac{l_F}{l} \quad \text{and} \quad \text{Da}_F = \frac{s_F}{\check{u}}\frac{l}{l_F},$$

where the suffix F is used to denote freely-propagating values. Specifically, freely-propagating flame simulations were conducted for range of equivalence ratios. Probability density functions of the local flame speed and width along an isotherm were used to derive a freely-propagating flame speed and width. We then performed simulations at fixed freely-propagating Karlovitz and Damköhler numbers in both the thin reaction zone and the distributed burning regime and demonstrated that scaling based on the freely-propagating values effectively eliminates the dependence on equivalence ration.

2. Computational Methodology

The simulations presented here are based on a low Mach number formulation of the reacting flow equations. The methodology treats the fluid as a mixture of perfect gases. We use a mixture-averaged model

for differential species diffusion and ignore Soret, Dufour, gravity and radiative transport processes. With these assumptions, the low Mach number equations for an open domain are

$$\frac{\partial(\rho \boldsymbol{u})}{\partial t} + \nabla \cdot (\rho \boldsymbol{uu}) = -\nabla \pi + \nabla \cdot \tau,$$

$$\frac{\partial(\rho Y_i)}{\partial t} + \nabla \cdot (\rho Y_i \boldsymbol{u}) = \nabla \cdot (\rho \mathcal{D}_i \nabla Y_i) - \dot{\omega}_i,$$

$$\frac{\partial(\rho h)}{\partial t} + \nabla \cdot (\rho h \boldsymbol{u}) = \nabla \cdot \left(\frac{\lambda}{c_p} \nabla h\right) +$$

$$\sum_i \nabla \cdot \left[h_i \left(\rho \mathcal{D}_i - \frac{\lambda}{c_p}\right) \nabla Y_i\right],$$

where ρ is the density, U is the velocity, Y_i is the mass fraction of species i, h is the enthalpy of the gas mixture, and $\dot{\omega}_i$ is the net destruction rate for species i due to chemical reactions. Also, λ is the thermal conductivity, τ is the stress tensor, c_p is the specific heat of the mixture, and $h_i(T)$ and $\mathcal{D}_i$ are the enthalpy and species mixture-averaged diffusion coefficients of species i, respectively where T denotes temperature. These evolution equations are supplemented by an equation of state for a perfect gas mixture.

The basic discretization combines a symmetric operator-split treatment of chemistry and transport with a density-weighted approximate projection method. The projection method incorporates the equation of state by imposing a constraint on the velocity divergence. The resulting system is integrated with time steps determined by the relatively slow advective transport. Advection is treated explicitly. Faster diffusion and chemistry processes are treated time-implicitly. This integration scheme is embedded in a parallel adaptive mesh refinement algorithm framework based on a hierarchical system of rectangular grid patches. The complete integration algorithm is second-order accurate in space and time, and discretely conserves species mass and enthalpy. The transport coefficients, thermodynamic relationships and hydrogen kinetics (chemical source terms) are obtained from the the GRIMech 2.11 model [14] with the relevant carbon species removed. The reader is referred to [15] for details of the low Mach number model and its numerical implementation, and to [16] for previous applications of this methodology to the simulation of premixed turbulent flames.

The overall numerical scheme is known to converge with second-order accuracy, and the ability of the scheme to perform direct numerical simulation was examined in [17]. The non-oscillatory finite-volume approach used remains stable even when under-resolved, and so some care is required to ensure that simulations are well-resolved. It was shown in [17] that a marginally resolved viscous simulation has an effective Kolmogorov length scale, η_e and effective viscosity that are slightly larger than that specified. Dimensional analysis was used to characterize the inviscid extreme, known as Implicit Large Eddy Simulation (ILES), through an analogy with the theory of [18]. From this analysis, an expression for the effective viscosity ν_e was obtained that describes the transition from well-resolved to pure ILES, $\nu_e = \nu_u + \nu_{\Delta x} \exp(-\nu_u/2\nu_{\Delta x})$, from which the effective Kolmogorov length scale can be derived where ($\nu_{\Delta x}$ is the effective viscosity of a simulation with a cell width Δx and zero diffusion, and ν_u is the physical viscosity. In the regime considered here, resolution of the turbulence places more stringent requirements on the simulation than does the chemistry. Detailed simulations, discussed in Aspden *et al.* [13] show the if $\eta_e/\eta < 1.5$, which is satisfied for the simulation presented here, then the turbulence is well-resolved.

3. Freely-Propagating Flames

To establish freely-propagating flame speeds and widths, a simulation was run for each equivalence ratio $\varphi = 0.31$, 0.34, 0.37 and 0.4. In each case, a downward-propagating flame was simulated in a domain with a 3cm square cross-section, and a height of 9cm. Uniform inflow was specified at the lower boundary, and the active control algorithm described in [19] was used to keep the flame at a statistically-steady height above the inlet. Lateral periodic boundaries were used, with outflow at the top of the domain. A base grid of $128 \times 128 \times 384$ was supplemented by two levels of refinement with refinement ratio 2, giving an effective resolution of $512 \times 512 \times 1536$, corresponding to a fine computational cell-width of approximately 59 microns, which was found to be adequate to resolve these lean hydrogen flames. Each simulation was initialized with a flat flame perturbed by a superposition of long wavelength Fourier modes. The flame was allowed to evolve without adaptive mesh refinement to allow the flame to become established at reduced expense. Refinement was then added to evolve a well-resolved statistically-steady flame to take the necessary measurements.

Figure 2 shows the temperature field on a two-dimensional vertical slice of a 3cm×3cm section of the freely-propagating flame simulation at an equivalence ratio of $\varphi = 0.40$. The thermodiffusive instability leads to the breakdown of the flat-laminar flame, resulting in the cellular burning structure clearly visible in figure 2. Hydrogen diffuses preferentially into the hot regions, which then burn more intensely than the flat laminar flame, resulting in the hot spots shown by the dark red patches. The inset shows the local burning rate, where the peak is around 4 times the flat laminar flame value.

The freely-propagating flames were analyzed following the approach of [10]. Data were sampled from several time points in each simulation. At each point, a flame surface was defined by finding an isotherm close to the temperature corresponding to the peak heat release in the flat laminar flame, and sections of the isotherm were removed where the burning rate was below some critical value. Integral volumes were constructed following gradients of temperature away

from the isotherm, forming a local flame coordinate system.

The local flame speed was evaluated by integrating the rate of hydrogen consumption over each integral volume, and normalizing by the hydrogen density times the cross-sectional area of the integral volume. Figure 3 shows joint probability density functions (JPDFs) of the local flame speed normalized by the flat laminar flame speed, against the mean curvature of the isotherm normalized by the flat laminar flame width, where the first moment has been taken with respect to the flame speed to eliminate the low level burning near the origin. Regions of positive curvature correspond to where the center of curvature is on the products side of the flame, which are associated with regions where the burning is enhanced by preferential diffusion of hydrogen. This highlights both the effect of the thermodiffusive instability on the local flame speed for low Lewis number flames, and importantly the consequential variation with equivalence ratio, both of which make the numerical study of the fundamentals of hydrogen combustion extremely challenging.

Freely-propagating values for flame speed and width were constructed using probability density functions (PDFs) of local flame speed, evaluated as above, and local flame width, evaluated by dividing the temperature jump across the flat laminar flame by the maximum temperature gradient along the normal to the isotherm. The PDFs were then be evaluated by sampling across the isotherms over the range of time points. Figure 4 shows the PDFs of the local flame speed and flame width along the flame front, normalized by the flat laminar flame values, where the first moment has been taken to remove the effects of the data near the origin. In each case, there is a clear peak, which corresponds to a predominant flame speed and width, which are both faster and thinner than the corresponding flat laminar flame. The resulting behavior of the thermodiffusive instability is a flame that burns more intensely in a thinner flame than in the flat laminar flame. The solid vertical lines denote the values that were assigned as the freely-propagating flame, which are given in table 1. The location of the peak in the local flame speed PDF is higher than the laminar flame speed, by a factor of approximately 2.1 for $\varphi = 0.4$ and approximately 4.8 for $\varphi = 0.31$. The location of the peak in the thermal thickness decreases in each case, by a factor of approximately 0.66 for $\varphi = 0.4$ and approximately 0.29 for $\varphi = 0.31$. It is this variation with φ that is responsible for the lack of generality in Ka_L and Da_L for lean hydrogen. The modified Karlovitz and Damköhler numbers for the slices shown in figure 1 are given in table 1, where each case is lower than the corresponding laminar value, increasingly so with decreasing φ.

4. Turbulent Flame Simulations

Turbulent flame simulations were run following the approach taken in [13, 20]. The active control algorithm is not well-suited to very high levels of turbulence, and so a high aspect ratio (8:1) domain was used, with a downward-propagating flame. Periodic lateral boundary conditions were specified, with a free-slip base and outflow at the top of the domain. The background turbulent velocity field was maintained following [13, 17, 20] using a source term in the momentum equations, consisting of a superposition of long-wavelength Fourier modes, resulting in a time-dependent zero-mean turbulent velocity field. It was demonstrated in [17] that this approach gives approximately 10 integral length scales across the domain. An inert calculation was run to establish the turbulence, and the reacting flow simulation was initialized by superimposing a laminar flame solution onto the turbulent velocity field. The base grid in each case was $64 \times 64 \times 256$, with two levels of refinement used once the flame had become established, giving an effective resolution of $256 \times 256 \times 2048$.

A new simulation was run at $\varphi = 0.40$ to match the conditions of case D31, where $Ka_F = 79$. Specifically $L \approx 17.2 l_F$ and $\check{u} \approx 6.8 s_F$. These cases will be referred to as L31 and L40, denoting the low Ka_F. Figure 5 compares two-dimensional slices of density, burning rate and temperature for the cases at $Ka_F = 79$ (note only five-eighths of domain height are shown). The peak temperatures are above the adiabatic flame temperatures, which indicates that there is focusing of hydrogen through differential diffusion, and that the flames are in the thin reaction zone, not in the distributed burning regime (this will be examined in more detail below). The two turbulent flames are clearly similar in structure; the turbulence tears off packets of fuel, but appears unable to disrupt the internal flame structure. The result is a sharp interface between fuel and products in both cases, and the burning occurs in small-scale structures over a broad flame brush.

Three further simulations were run at $\varphi = 0.31$, 0.34 and 0.37 to match the conditions of D40, where $Ka_F = 410$. Specifically, $L \approx 7.6 l_F$ and $\check{u} \approx 50 s_F$. These cases will be referred to as H31-H40, denoting the high Ka_F. Figure 6 compares the slices of density, burning rate and temperature for the four cases. Density and temperature have been normalized by the laminar values, and the burning rate has been normalized by six times the peak laminar burning rate. Again, the turbulent flames appear similar to each other in structure (and distinctly different to the two simulations at $Ka_F = 79$), resembling a distributed flame. It is possible to normalize the slices by the laminar values because the burning is in the distributed regime. When mixing is predominantly due to turbulence, the values of temperature, for example, remain between the cold fuel and adiabatic flame temperatures. Each case consists of a single turbulently-broadened flame, and there is no longer a sharp interface between the fuel and the products. At the lowest equivalence ratio $\varphi = 0.31$, the flame appears to be significantly broader than at the the other three equivalence ratios, although there is a slight decreas-

ing trend in the turbulent flame width as equivalence ratio increases. Although the turbulent flames do not appear to be identical, the normalization by freely-propagating values appears to have made a vast improvement over normalization by flat laminar flame values.

To demonstrate further that the turbulent flame behavior is matched better using the freely-propagating values, two diagnostics will be presented following [13]. Specifically, PDFs of $|\nabla\rho|$ are used to characterize turbulent mixing of the density field, and JPDFs of fuel mole fraction and temperature are used to show that the $\mathrm{Ka}_F = 79$ and $\mathrm{Ka}_F = 410$ cases are in different burning regimes.

Aspden *et al.* [13] showed that when turbulence was the dominant mixing process, the normalized PDF of $|\nabla\rho|$ was close to exponential in distribution, which is a well-known characteristic of turbulent scalar mixing, see [21–23] as examples). When the turbulence did not disrupt the internal flame structure, the normalized PDF presented more rapid decay than exponential. Figure 7 shows PDFs of normalized by the respective standard deviation for (a) cases L31, L40, and H31-H40. The solid black line denotes a normalized exponential decay. The data have been conditioned such that only regions where the density is between 10% and 90% of the laminar extremes contribute to the PDF. The distributions of L31 and L40 are both similar to each other, and present more rapid decay than exponential, indicative of burning in the thin reaction zone. The distributions of H31-H40 are also similar to each other and close to exponential, indicative of burning in the distributed burning regime.

Figure 8 shows JPDFs of fuel mole fraction against temperature for cases L40 and H37 (the reader is referred to [13] for comparison with L31 and H40). The solid lines denote the laminar flat flame distributions (red for $\varphi = 0.31$, through black for $\varphi = 0.49$). The $\mathrm{Ka}_F = 79$ cases show a broad distribution that is between the laminar flame and a linear distribution. In the $\mathrm{Ka}_F = 410$ cases, the JPDFs present narrow distributions distinct from the laminar flame distributions and close to linear. This demonstrates that species and thermal diffusion are playing a much reduced role compared with turbulent mixing. The $\mathrm{Ka}_F = 79$ cases are similar to each other and typical of the thin reaction zone, and the $\mathrm{Ka}_F = 410$ cases are all similar to each other and typical of the distributed burning regime.

5. Discussion and Conclusions

For thermodiffusively-unstable low Lewis number flames, the freely propagating flame structure is significantly different than the idealized flat laminar flame, undermining the standard approach of characterizing turbulent flames in terms of Karlovitz and Damköhler numbers based on flat laminar flame properties. This was found to be a particular problem in the turbulent flame study of [13] (see figure 1), where turbulent flames at the same (laminar)

Karlovitz and Damköhler number presented distinctly different behavior. In this paper, we have proposed an approach to rectify this shortcoming by measuring freely-propagating flame properties, thereby accounting for the flame response to its inherent instability in three dimensions. This was achieved through high-resolution three-dimensional simulations of lean premixed hydrogen flames at a variety of equivalence ratios, using the active control algorithm of [10]. The difficulties associated with studying low Lewis number flames were highlighted through joint probability density functions of local flame speed with curvature. Probability density functions for flame speeds and widths local to a flame surface based on an isotherm were used to assign freely-propagating flame properties. Reevaluation of the Karlovitz numbers showed that in the leanest case Ka_L was almost 20 times Ka_F. Furthermore, Ka_F in the two extreme cases ($\varphi = 0.31$ and 0.40) differed by a factor of approximately 5.2. New simulations were run to match the freely-propagating Karlovitz and Damköhler numbers across the range of equivalence ratios. Conditions were chosen to match those of case D31 at $\mathrm{Ka}_F = 79$ using an equivalence ratio of $\varphi = 0.40$, and case D40 at $\mathrm{Ka}_F = 410$ using equivalence ratios of $\varphi = 0.31$, 0.34, and 0.37. At $\mathrm{Ka}_F = 79$, a similar turbulent response was observed in both flames, where the turbulence was only able to tear the flame and the flame burned in small structures over a broad flame brush. The normalized probability density function of $|\nabla\rho|$ decayed more rapidly than exponential, and the joint probability density function of fuel mole fraction against temperature presented a broad distribution, both of which are characteristics of flames in the thin reaction zone. At $\mathrm{Ka}_F = 410$, the flames were once again similar to each other, and different than the $\mathrm{Ka}_F = 79$ flames. The PDFs of $|\nabla\rho|$ were close to exponential in distribution, and the JPDFs of fuel mole fraction against temperature collapse to a narrow distribution close to linear, both of which are indicative of burning in the distributed regime.

References

[1] G. H. Markstein, *The Journal of Chemical Physics* 17 (4) (1949) 428–429.
[2] Y. B. Zeldovich, *Theory of Combustion and Detonation in Gases (in Russian)*, Acad. Sci. USSR, 1944.

[3] B. Bregeon, A. S. Gordon, F. A. Williams, *Combustion and Flame* 33 (1978) 33–45.

[4] T. Mitani, F. A. Williams, *Combust. Flame* 39 (1980) 169–190.

[5] B. Bedat, R. K. Cheng, *Combust. flame* 100 (1995) 485–494.

[6] D. Littlejohn, R. K. Cheng, *Proceedings of the Combustion Institute* 31 (2) (2007) 3155 – 3162.

[7] R. K. Cheng, D. Littlejohn, P. A. Strakey, T. Sidwell, *Proceedings of the Combustion Institute* 32 (2) (2009) 3001 – 3009.

[8] M. Baum, T. J. Poinsot, D. C. Haworth, N. Darabiha, *J. Fluid Mech.* 281 (1994) 1–32.

[9] J. B. Bell, R. K. Cheng, M. S. Day, I. G. Shepherd, *Proc. Combust. Inst.* 31 (2007) 1309–1317.

[10] M. S. Day, J. B. Bell, P.-T. Bremer, V. Pascucci, V. Beckner, M. J. Lijewski, *Combustion and Flame* 156 (5) (2009) 1035 – 1045.

[11] M. S. Day, J. B. Bell, R. K. Cheng, S. Tachibana, V. E. Beckner, M. J. Lijewski, in: *SciDAC, Journal of Physics: Conference Series*, Vol. 180, Institute of Physics Publishing, 2009, p. 012031.

[12] P. Strakey, T. Sidwell, J. Ontko, *Proc. Comb. Inst.* 31 (2007) 3173–3180.

[13] A. J. Aspden, M. S. Day, J. B. Bell, *In preparation.* Available at ccse.lbl.gov.

[14] C. T. Bowman, *GRI-Mech 2.11*, available at http://www.me.berkeley.edu/gri_mech.

[15] M. S. Day, J. B. Bell, *Combust. Theory Modelling* 4 (2000) 535–556.

[16] J. B. Bell, M. S. Day, J. F. Grcar, *Proc. Combust. Inst.* 29 (2002) 1987–1993.

[17] A. J. Aspden, N. Nikiforakis, S. B. Dalziel, J. B. Bell, *Comm. App. Math. Comput. Sci.* 3 (1) (2008b) 101.

[18] A. N. Kolmogorov, *Royal Society of London Proceedings Series A* 434 (1991) (a) 9–13, and (b) 15–17.

[19] J. B. Bell, M. S. Day, J. F. Grcar, M. J. Lijewski, *Comm. App. Math. Comput. Sci.* 1 (1) (2005) 29–52.

[20] A. J. Aspden, J. B. Bell, M. S. Day, S. E. Woosley, M. Zingale, *The Astrophysical Journal* 689 (2008a) 1173–1185.

[21] J. P. Gollub, J. Clarke, M. Gharib, B. Lane, O. N. Mesquita, *Phys. Rev. Lett.* 67 (25) (1991) 3507–3510.

[22] Jayesh, Z. Warhaft, *Phys. Rev. Lett.* 67 (25) (1991) 3503–3506.

[23] S. T. Thoroddsen, C. W. Van Atta, *Journal of Fluid Mechanics* 244 (1992) 547–566.

φ	0.31	0.34	0.37	0.40
s_L, cm/s	4.68	9.34	15.2	22.4
l_L, mm	1.9	1.1	0.79	0.63
s_F, cm/s	22.6	32.8	38.9	47.4
l_F, mm	0.55	0.47	0.44	0.41
Case	D31	D34	D37	D40
$\breve{u}$, m/s	5.0	9.98	16.3	23.9
l, mm	0.95	0.55	0.395	0.314
L, mm	9.5	5.5	3.95	3.14
Ka_L	1560	1560	1560	1560
Da_L	4.7e-3	4.7e-3	4.7e-3	4.7e-3
Ka_F	79	155	284	410
Da_F	7.8e-2	3.9e-2	2.2e-2	1.5e-2
Case	H31	H34	H37	L40
$\breve{u}$, m/s	11.4	16.5	19.6	10.5
l, m	0.42	0.36	0.33	0.71
L, m	4.2	3.6	3.3	7.1
Ka_L	8080	4105	2257	302
Da_L	9e-4	1.9e-3	3.2e-3	2.4e-2
Ka_F	410	410	410	79
Da_F	1.5e-2	1.5e-2	1.5e-2	7.8e-2
Δx, μm	16	14	13	28
η, μm	6.5	4.7	4.1	19
η_e, μm	8.1	6.4	5.7	20

Table 1: Simulation properties.

List of Figure Captions

Figure 1. (233 words – double column) Two-dimensional slices of three-dimensional simulations of lean-premixed hydrogen for cases D31-D40.

Figure 2. (134 words) Temperature slice of a 3cm×3cm section of the freely-propagating flame simulation at $\varphi = 0.40$. The inset shows the burning rate, where the peak burning rate is approximately 4 times that of the flat laminar flame.

Figure 3. (242 words) Joint probability density function of normalized burning rate against normalized mean curvature, where the first moment has been taken with respect to the burning rate.

Figure 4. (240 words) First moments of the probability density functions for normalized local flame speed (top) and width (bottom) for the freely-propagating flames.

Figure 5. (123) Two-dimensional slices of density, burning rate and temperature for cases L31 and L40.

Figure 6. (260 words – 2 column) Two-dimensional slices of density, burning rate and temperature for cases H31-H37. The density and temperature have been normalized by the corresponding laminar values, and the burning rate has been normalized by six times the peak laminar burning rate.

Figure 7. (112 words) PDFs of $|\nabla\rho|$ for the turbulent flames.

Figure 8. (233 words) JPDFs of fuel mole fraction against temperature for cases L40 and H37.

Total words from text: $4 \times 900 + 326 = 3926$

Total length from figures (including doubles): 1577 words

Length of table: 222 words

Total word count (Method 2): 3926 + 1577 + 222 = 5725
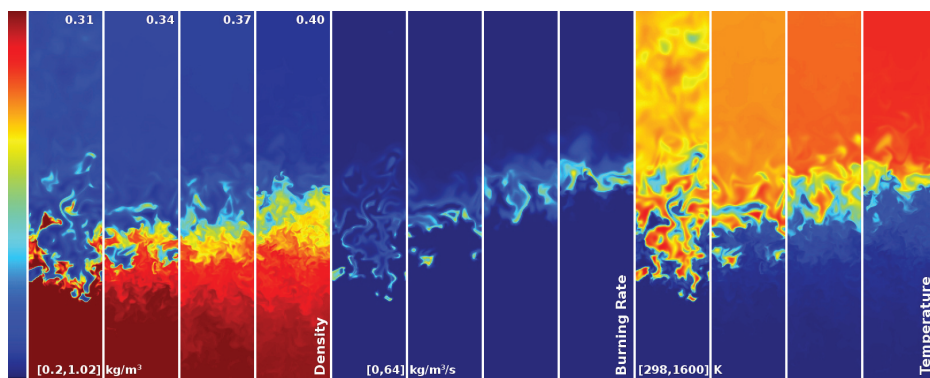
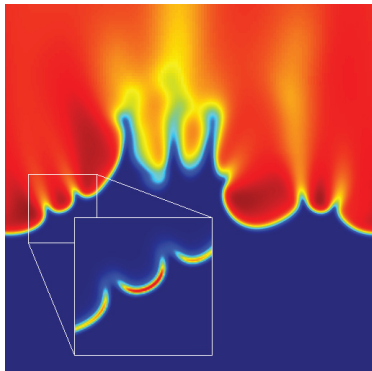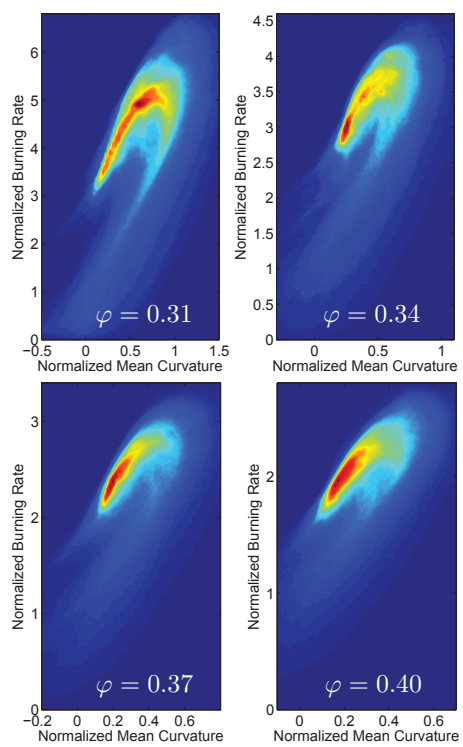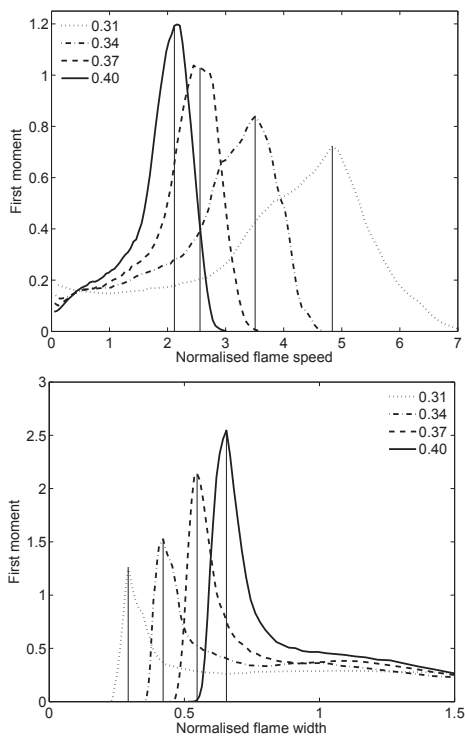Fig. 1: Two-dimensional slices of three-dimensional simulations of lean-premixed hydrogen for cases D31-D40.

Fig. 2: Temperature slice of a 3cm×3cm section of the freely-propagating flame simulation at $\varphi = 0.40$. The inset shows the burning rate, where the peak burning rate is approximately 4 times that of the flat laminar flame.

Fig. 3: Joint probability density function of normalized burning rate against normalized mean curvature, where the first moment has been taken with respect to the burning rate.

Fig. 4: First moments of the probability density functions for normalized local flame speed (top) and width (bottom) for the freely-propagating flames.
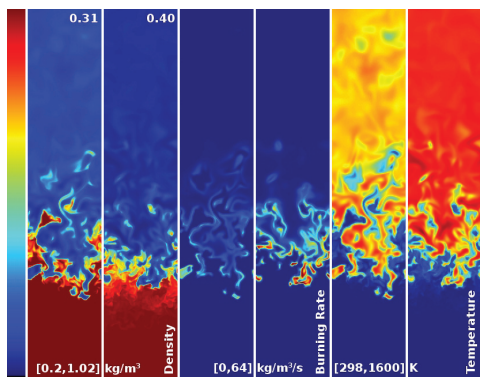
Fig. 5: Two-dimensional slices of density, burning rate and temperature for cases L31 and L40.
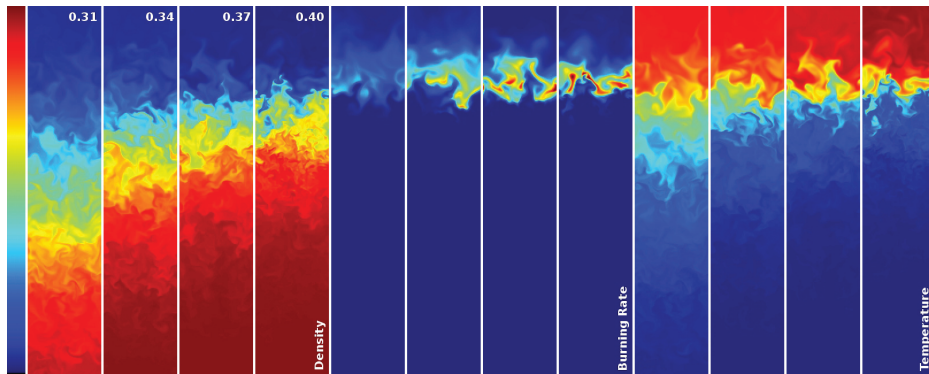
Fig. 6: Two-dimensional slices of density, burning rate and temperature for cases H31-H37. The density and temperature have been normalized by the corresponding laminar values, and the burning rate has been normalized by six times the peak laminar burning rate.
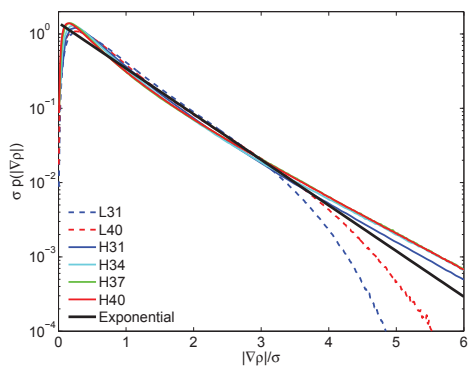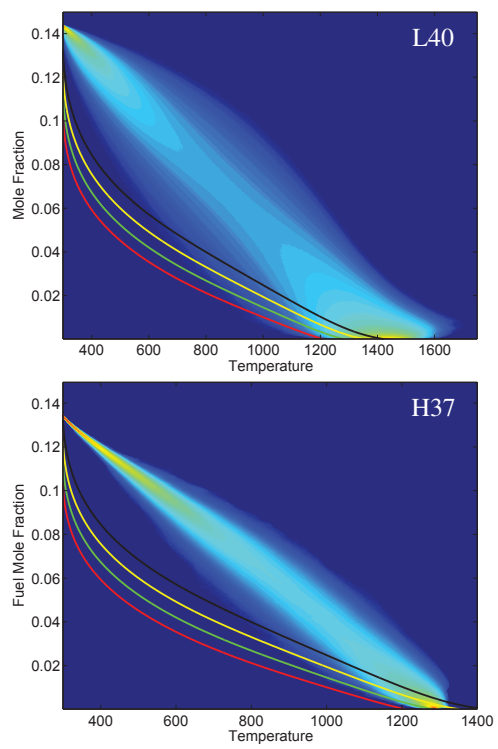
Fig. 7: PDFs of $|\nabla\rho|$ for the turbulent flames.

Fig. 8: JPDFs of fuel mole fraction against temperature for cases L40 and H37.